International Journal of Sciences and Techniques of Automatic control & computer engineering
IJ-STA, Special Issue, CEM, December 2008, pp. 636–651.

The Classical and Analytic DTC for Photovoltaic Panel Position and Control

Badii Bouzidi, Abderrazak Yangui and Fatma Ben Salem

Research Unit on Renewable Energies and Electric Vehicles
University of Sfax, Sfax Engineering School, BP W, 3038 Sfax, Tunisia
e-mails: badiibouzidi2010@yahoo.fr, abderrazak.yangui@enis.run.tn
fatma.bensalem@enis.rnu.tn

Abstract: *In this paper, an approach consisting in moving photovoltaic panels according to the maximum sunshine position in order to extract a high efficiency is proposed. Firstly, the model of the photovoltaic generator is described. Secondly the designed maximum sunshine position tracking system is presented and experimental results consisting of no-load voltage variations during different periods of the year are described. Finally, a comparison study between three direct torque control (DTC) strategies dedicated for the maximum sunshine position tracking system is carried out. It has been found that the three DTC strategies exhibit high dynamic performance. However, these strategies are more or less penalized by some drawbacks such as demagnetization, high commutation frequency and high torque ripples.*

Keywords: *Induction motor, maximum sunshine position tracking system, experimental Tests, direct torque control, look-up table, demagnetization, torque ripple, commutation frequency.*

1. Introduction

The low efficiency of photovoltaic systems which is party due to the fluctuation of solar radiation especially with the panels exposed to the sun in a fixed position represents one of the drawbacks of such systems. In order to extract a maximum power during the day and therefore a high efficiency of photovoltaic systems, an approach consisting in moving the photovoltaic panels according to the maximum sunshine position has been proposed in [11]. The maximun sunshine tracking system offers an energy increase of almost 30 to 40% [9]. To do so, an electric motor drive could be associated to the photovoltaic panels in order to be able to track the maximum sunshine positions during the day. Accounting for the high perturbation amplitude applied to the panel, the control strategy to be implemented in the drive is of great importance. Introduced by *Takahashi* and by *Depenbrock* [1, 2] since 1985, the direct torque control (DTC) has been selected in order to fulfill the considered application requirements, especially a maximum torque at standstill. In what follows the paper is organized in four sections. The first one describes the model of the

This paper was recommended for publication in revised form by the editor Staff.
Edition: CPU of Tunis, Tunisia, ISSN: 1737-7749

photovoltaic generator. The second section presents the developed maximum sunshine position tracking system. Then, experimental results carried out on the developed system are provided. These represent a data base which yields the variation of the no-load voltage of three photovoltaic panel records during different periods of the day and for different positions. The third section deals with the basis of the direct torque control (DTC) strategy and its application to the control of the developed maximum sunshine position tracking system. Within this, three DTC strategies are considered. The last section is devoted to a comparative study between the performance of the three DTC strategies considered in the previous section. The major comparison criteria are: (i) the reduction of the demagnetization phenomenon, (ii) the reduction of the torque ripples and (iii) the reduction of the inverter commutation frequency.

2. Solar Cell Features Versus Solar Radiation and Temperature

The basic model of a photovoltaic cell, is shown in Figure1 [10]. A photovoltaic generator composed of N_s series connected cells and N_p parallel-connected modules presents a non linear output characteristics which is expressed as follows [8, 10, 7]:

$$I_p = N_p I_{ph} - N_p I_s \left[exp\left(\frac{A}{N_s} \left[V_p + R_s I_p \right] \right) - 1 \right] - \left(\frac{V_p + R_s I_p}{R_{sh}} \right) \quad (1)$$

where V_p and I_p are the output voltage and the output current, respectively, I_{ph} and I_s are the cell photo-current and the reverse saturation current, respectively, R_s and R_{sh} are the cell series resistance and the cell shunt resistance, respectively, and A is the thermal voltage depending on the cell temperature, such that $A = \frac{q}{nKT}$, q is the electronic charge, K is the *Boltzmann* constant and n is the ideality factor.

Let us consider the expression of the cell photo-current I_{ph} in terms of the temperature T and the solar irradiance which is given by equation(2) [12]:

$$I_{ph} = \frac{E}{100} \left[I_{cc} + K_1 \left(T - 298 \right) \right] \quad (2)$$

where E is the solar irradiation $\left[\frac{\mathrm{mW}}{\mathrm{cm}^2}\right]$, and T and T_r are the cell temperature [K] and the reference temperature [K], respectively, I_{cc} is the short circuit current at T_r, and K_1 is the short circuit current temperature coefficient $\left[\frac{\mathrm{A}}{^\circ\mathrm{C}}\right]$.

The reverse saturation current I_s is given by the following equation [12]:

$$I_s = I_{sref} + \left(\frac{T^3}{T_r^3} \right) exp\left[\left(\frac{qE_q}{nK} \right) \left(\frac{1}{T_r} - \frac{1}{T} \right) \right] \quad (3)$$

where I_{sref} is the reverse saturation current at T_r and E_q is the material band gap energy.

Giving the fact that R_{sh} is generally omitted as far as it is much greater than R_s, then equation 1 is reduced to [10, 12]:

$$I_p = N_p I_{ph} - N_p I_s \left[exp\left(\frac{A}{N_s} \left[V_p + R_s I_p \right] \right) - 1 \right] \quad (4)$$

Under no-load operation ($I_p = 0$), the expression of the open circuit voltage (no-load voltage) V_{po} is as follows [5, 8]:

$$V_{po} = \frac{N_s KT}{q} ln\left(\frac{N_p I_{ph}}{N_p I_s} + 1\right) \quad (5)$$

An approach to the identification of the parameters required for the determination of the output characteristic (current-voltage) has been proposed by *Chenni* [12].

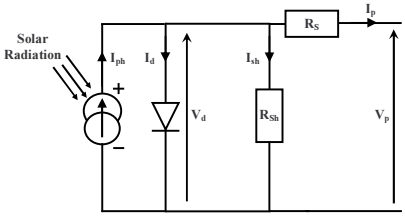

Figure 1: PV solar cell equivalent circuit.

The variations of the current and of the power versus the voltage of a commercial PV module (see table 1) at different values of the temperature and different levels of solar irradiation are illustrated in figure 2.(a) and(b), respectively. It can be seen from figure 2.(b) that the output current varies greatly with the solar irradiation changes, which is not the case of the output voltage. The output power increases with an increase of the solar irradiation. Indeed, the photo-current (hence, the short circuit current), is a linear function of the solar irradiation while the open-circuit voltage is a logarithmic function of the solar irradiation. Figure 2.(a) shows that on one hand the open-circuit voltage decreases with an increase of the cell temperature, which is due to a sharp increase of the reverse saturation current, and on the other hand a slight increase of the short-circuit current. This is said, one can notice a decrease of the output power versus the cell temperature. Accounting for the high nonlinearity of the above-described characteristics, it turns to be interesting to increase the output power by tracking the maximum sunshine position which is considered in the present work.

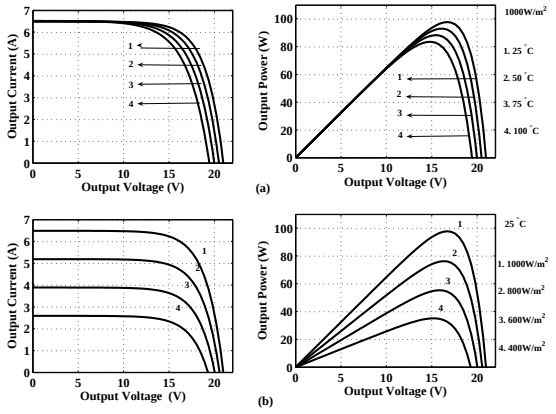

Figure 2: Characteristics of a PV module : (a) constant irradiation and varying temperature and (b) constant temperature and varying irradiation.

Table 1: Specifications of Siemens solar panels(manufactured by SHELL SOLAR).

Rated power	100[W]	K_1	410^{-4} $[\frac{A}{^\circ C}]$
Short circuit current	6 $[A]$	Current at maximum power	5.9 $[A]$
Open circuit voltage	21 $[V]$	Voltage at maximum power	17 $[V]$
Series connected cells	72	Parallel connected modules	1

3. Maximum Sunshine Position Tracking System

A new maximum sunshine position tracking system has been proposed in [11]. It consists of an experimental set which allows the displacement of three photovoltaic panels within latitudes and meridians. Figure 3 shows the Layout of the proposed tracking system driven by an induction motor under DTC, where (a) gives a front view and (b) gives a rear view. The developed maximum sunshine position tracking system is intended to assess as accurately as possible the location of the sun with respect to earth during the day. The designed tracking system has two freedom degrees in such a way that it allows the displacement of the photovoltaic system within latitudes and meridians:

- the first degree of freedom is controlled automatically by an induction motor drive under the control of a DTC strategy. It allows the rotation of the photovoltaic panels with an angle which varies between -60° and 60°. The 0° angle corresponds to an horizontal position of the photovoltaic panels. Positive angles are allocated to the east orientation of the photovoltaic panels. Negative angles are allocated to the west orientation of the photovoltaic panels. The variation of this angle is carried out in order to determine the maximum sunshine position tracking during the day,
- the second degree of freedom is time-to-time achieved manually according to the period of the year. To do so, three suitable positions have selected taking into account of the geographical site in which is located the photovoltaic panels. Such a sited is characterized by four seasons during a year. Hence the position variation within this axis can be adjusted only three times during the year. This degree of freedom allows the variation of the declination angle of the photovoltaic panels from -10° to 50°.

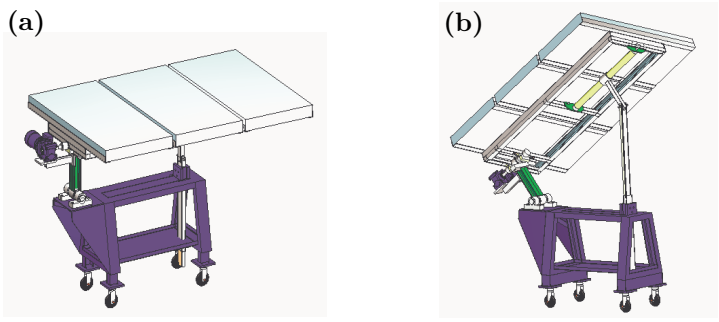

Figure 3: Layout of the proposed maximum sunshine position tracking system. **Legend**: (a) front view, (b) rear view.

Experimental Tests

Three photovoltaic panels are fixed on the developed maximum sunshine position tracking. Then experiments have been carried out in the suburb of Sfax (Tunisia) during March and April, every day from 9 AM to 5 PM. These tests consisted on varying the orientation angle of the panels from -50 to 50 degrees, at the beginning of each hour, and measuring the resulting no-load voltage every 10 degrees. Doing so, we have generated a data base that has been used for the resolution of the problem of tracking of the maximum sunshine position. The position corresponding to the maximum sunshine is the one in which the maximum no-load voltages are provided by the photovoltaic panels.Referring to equation (5), we can notice that the no-load voltage increases with a logarithmic increase of the cell photo-current I_{ph} which is proportional to the solar radiation. Therefore, the no-load voltage rises with the increase of the solar radiation. Figure 4 shows 3D plots of the no-load voltage versus the orientation angle and the day time. One can notice that:

- for each hour there is a position which corresponds to the maximum of no-load voltage,
- the no-load voltage versus the angle at a given day time presents a parabolic shape,
- when day time increases, the angle corresponding to the maximum no-load voltage moves following the sun position.

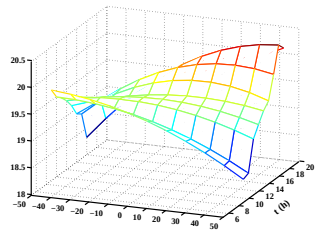

Figure 4: 3D plots of the no-load voltage versus the orientation angle and the time.

4. Control of the Maximum Sunshine Position Tracking System

Accounting for the perturbations applied to the maximum sunshine position tracking system, it is of great importance to select a suitable control strategy to be implemented in the induction motor drive. Following a comparative study, the direct torque control (DTC) strategy has been selected. The principle of DTC strategies consists of describing the way in which the stator flux and the torque are directly controlled by selecting a suitable inverter's voltage vector. DTC strategies have been commonly implemented in induction motor drives.
The dynamic behavior of an induction machine is described in terms of space vectors variables as follows:

$$\begin{cases} v_{\alpha s} &= r_s i_{\alpha s} + \frac{d}{dt}\phi_{\alpha s} \\ v_{\beta s} &= r_s i_{\beta s} + \frac{d}{dt}\phi_{\beta s} \\ 0 &= r_r i_{\alpha r} + \frac{d}{dt}\phi_{\alpha r} + \omega_m \phi_{\beta r} \\ 0 &= r_r i_{\beta r} + \frac{d}{dt}\phi_{\beta r} - \omega_m \phi_{\alpha r} \end{cases} \quad (6) \qquad \begin{cases} \phi_{\alpha s} &= l_s i_{\alpha s} + M i_{\alpha r} \\ \phi_{\beta s} &= l_s i_{\beta s} + M i_{\beta r} \\ \phi_{\alpha r} &= M i_{\alpha s} + l_r i_{\alpha r} \\ \phi_{\beta r} &= M i_{\beta s} + l_r i_{\beta r} \end{cases} \quad (7)$$

The voltage vector of the inverter feeding the induction motor is expressed as:

$$\overline{V}_s = \sqrt{\frac{2}{3}}\left[S_a + S_b e^{j\frac{2\pi}{3}} + S_c e^{j\frac{4\pi}{3}}\right] \quad (8)$$

where S_a, S_b and S_c are the inverter switching functions, which takes a logical value (1 or 0).

The stator flux vector is given by the following:

$$\overline{\Phi}_s = \overline{\Phi}_{s0} + \int_0^t (\overline{V}_s - R_s \overline{I}_s) dt \quad (9)$$

Now, if the voltage drop across the stator resistance is neglected, equation (9) turns to be: $\Delta\overline{\Phi}_s = \overline{\Phi}_s(K+1) - \overline{\Phi}_s(K) \simeq \overline{V}_s T_s$ (10)

where T_s is the sampling period.

The stator flux amplitude and phase are expressed as follows:

$$\begin{cases} |\overline{\Phi}_s| &= \sqrt{\phi_{\alpha s}^2 + \phi_{\beta s}^2} \\ \theta_s &= arctan\left(\frac{\phi_{\beta s}}{\phi_{\alpha s}}\right) \end{cases} \quad (11)$$

Electromagnetic torque can be expressed in terms of stator current and flux as:

$$T_{em} = N_P\left(\phi_{\alpha s} i_{\beta s} - \phi_{\beta s} i_{\alpha s}\right) \quad (12)$$

where N_P is the pole pair.

4.1 Takahashi Basic DTC Strategy

The implementation scheme of a DTC based position regulation of an induction motor is shown in figure 5. The error between the reference position θ_m^* and the measured one θ_m is applied to the position regulator (P type) whose output provides the reference speed Ω_m^*. This latter is compared to the measured speed Ω_m. The obtained error is applied to the speed regulator (P.I. type) whose output provides the reference electromagnetic torque T_{em}^*. The estimated stator flux Φ_s and electromagnetic torque T_{em} are compared to the corresponding references. The errors are applied to the stator flux and torque bang-bang regulators, respectively. The outputs of the stator flux and torque regulators and the phase of the stator flux θ_s are applied to the vector selection table which generates the convenient combinations of the states of the inverter power switches. There are eight switching combinations, two of which yield zero voltage vectors. The voltage vectors, delivered by a 2-level inverter are shown in Figure 6. The output c_ϕ of the stator flux two-level hysteresis regulator takes "1" to increase ϕ_s and "-1" to decrease it. While the output c_τ of the torque 3-level hysteresis regulator takes "1" to increase T_{em}, "-1" to decrease it, and "0" to maintain it. The set of combinations of the power switch states considered in the *Takahashi* DTC basic strategy is given in table 2.

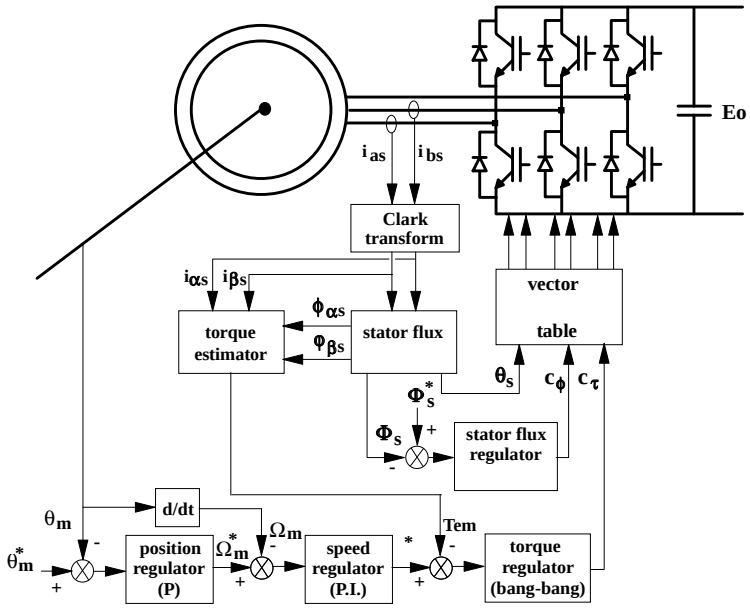

Figure 5: Induction motor position regulation based on DTC strategy.

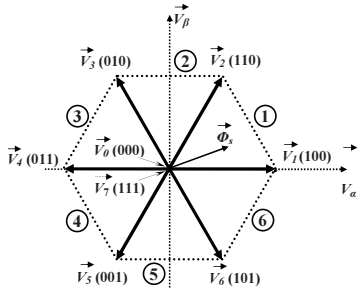

Figure 6: Switching-voltage space vectors.

Table 2: Look-up table of the *Takahashi* basic DTC strategy.

c_ϕ	+1			-1		
c_τ	+1	0	-1	+1	0	-1
S_1	V_2	V_7	V_6	V_3	V_0	V_5
S_2	V_3	V_0	V_1	V_4	V_7	V_6
S_3	V_4	V_7	V_2	V_5	V_0	V_1
S_4	V_5	V_0	V_3	V_6	V_7	V_2
S_5	V_6	V_7	V_4	V_1	V_0	V_3
S_6	V_1	V_0	V_5	V_2	V_7	V_4

Accounting for the load torque expression given by the following expression:

$$T_l = Ksin(\theta) \tag{13}$$

The Takahashi basic DTC strategy considers that the voltage drop across the statance resistance is negligible. This hypothesis is no longer true under low speed operation which is the case of the treated application. In this case, applying a zero voltage vector yields the following equation:

$$\Delta\overline{\Phi}_s = \overline{\Phi}_s(K+1) - \overline{\Phi}_s(K) = -R_s\overline{I}_s \tag{14}$$

which leads to a decrease of the stator flux. Therefore, it is expected that the Takahashi basic DTC strategy would be penalized by a demagnetization problem when implemented in the induction motor drive to control the maximum sunshine position tracking system.

4.2 Modified Takahashi DTC Strategy

In order to overcome the problem of demagnetization caused by zero voltage vectors included in the *Takahashi* basic DTC look-up table, the zero voltage vectors have been substituted by suitable active vectors. For a given stator flux vector and when the torque regulator output is "0", the active vector around which is located the sector including the stator flux vector extremity is applied. The resulting look-up table is given in table 3 [4]. It is obvious that the substitution of the zero-voltage vectors by active ones allows the elimination of the demagnetization problem. Nevertheless, this substitution is associated with an other crucial problem: that is an increase of the average inverter switching frequency which compromises the drive efficiency. In what follows, a third DTC strategy is considered in an attempt to solve both demagnetization and high average commutation frequency problems.

Table 3: Look-up table with zero-voltage vectors substituted by active ones.

c_Φ	+1	+1	+1	-1	-1	-1
c_τ	+1	0	-1	+1	0	-1
N_1	V_2	V_1	V_6	V_3	V_4	V_5
N_2	V_3	V_2	V_1	V_4	V_5	V_6
N_3	V_4	V_3	V_2	V_5	V_6	V_1
N_4	V_5	V_4	V_3	V_6	V_1	V_2
N_5	V_6	V_5	V_4	V_1	V_2	V_3
N_6	V_1	V_6	V_5	V_2	V_3	V_4

4.3 Analytically Based DTC Strategy

Referring to table 1, it is to be noted that zero-voltage sequences are systematically applied to the inverter when the torque has to be kept at it current value ($c_\tau = 0$). This represents a crucial limitation of *Takahashi* DTC strategy, in so far as during sequences where $c_\tau = 0$ the flux should be normally adapted according to c_ϕ, which is ignored through the application of zero-voltage sequences. Furthermore, some questions arise while analyzing *Takahashi* DTC strategy, for instance: why should we consider just two state hysteresis regulator to control

the stator flux? Why zero-voltage sequences are limited to $c_\tau = 0$? Would it be possible to reach better performances considering zero-voltage sequences while $c_\tau = -1$ or $+1$? etc. In order to be able to answer these questions, it is necessary to go further the empirical approach introduced by *Takahashi*. Within this, we have considered an analytical approach, proposed in [3, 6], which is based on the torque transient behavior taking into account different operating modes (including generator operation during braking).

4.3.1 Electromagnetic Torque Analysis

Let us consider the electromagnetic torque expression (12), and let us calculate its derivative:

$$\frac{d}{dt}T_{em} = N_p\left[\left(\phi_{\alpha s}\frac{d}{dt}i_{\beta s} - \phi_{\beta s}\frac{d}{dt}i_{\alpha s}\right) + \left(i_{\beta s}\frac{d}{dt}\phi_{\alpha s} - i_{\alpha s}\frac{d}{dt}\phi_{\beta s}\right)\right] \tag{15}$$

Accounting for equations (6) and (7); expression (15) turns to be:

$$\begin{aligned}\frac{d}{dt}T_{em} = N_p\Bigg[&v_{\alpha s}\left(i_{\beta s} - \frac{\phi_{\beta s}}{\sigma l_s}\right) - v_{\beta s}\left(i_{\alpha s} - \frac{\phi_{\alpha s}}{\sigma l_s}\right)\\ &-\frac{R_{sr}}{\sigma l_s N_p}T_{em} - \frac{\omega_m}{\sigma l_s}\Phi_s^2 + \omega_m\left(\phi_{\alpha s}i_{\alpha s} + \phi_{\beta s}i_{\beta s}\right)\Bigg]\end{aligned} \tag{16}$$

where $R_{sr} = r_s + \frac{l_s}{l_r}r_r$, $\sigma = 1 - \frac{M^2}{l_s l_r}$.

If the leakage flux is neglected, that is to say :

$$\begin{cases} l_s\sigma_s i_{\alpha s} << \phi_{\alpha s} \\ l_s\sigma_s i_{\beta s} << \phi_{\beta s} \end{cases} \tag{17}$$

then expression (16) is reduced to :

$$\frac{d}{dt}T_{em} = N_p\left[v_{\beta s}\frac{\phi_{\alpha s}}{\sigma l_s} - v_{\alpha s}\frac{\phi_{\beta s}}{\sigma l_s} - -\frac{R_{sr}}{\sigma l_s N_p}T_{em} - \frac{\omega_m}{\sigma l_s}\Phi_s^2\right] \tag{18}$$

In the case of zero-voltage ($v_{\alpha s} = v_{\beta s} = 0$), expression (18) turns to be:

$$\frac{d}{dt}T_{em} \simeq -\frac{R_{sr}}{\sigma l_s}T_e m - \frac{\Phi_s^2}{\sigma l_s}\Omega_m \tag{19}$$

In motor operation, Ω_m and T_{em} have the same signs, yielding domains D_{m1} and D_{m2} located in the (Ω_m,T_{em}) plane shown in figure 7, with:

$$\begin{cases} \frac{d}{dt}T_{em} < 0 \quad \text{if} \quad \Omega_m > 0 \quad (D_{m1}) \\ \frac{d}{dt}T_{em} > 0 \quad \text{if} \quad \Omega_m < 0 \quad (D_{m2}) \end{cases} \tag{20}$$

In generator operation, Ω_m and T_{em} have opposites signs, giving 4 domains D_{g1}, D_{g2}, D_{g3}, D_{g4}, with:

$$\begin{cases} \frac{d}{dt}T_{em} = 0, \quad T_{em} = -\frac{\Phi_s^2}{R_{sr}}\Omega_m \\ \frac{d}{dt}T_{em} < 0, \quad T_{em} > -\frac{\Phi_s^2}{R_{sr}}\Omega_m \quad (D_{g1}\ \&\ D_{g3}) \\ \frac{d}{dt}T_{em} > 0, \quad T_{em} < -\frac{\Phi_s^2}{R_{sr}}\Omega_m \quad (D_{g2}\ \&\ D_{g4}) \end{cases} \tag{21}$$

Accounting for the previous formulation, we can notice that:

- when the torque variation with respect to time is positive (domains: D_{m2}, D_{g2}, D_{g4}), applying a zero-voltage sequence yields an increase of torque,
- when the torque variation with respect to time is negative (domains: D_{m1}, D_{g1}, D_{g3}), applying a zero voltage sequence yields a decrease of torque.

These remarks are completely in disagreement with *Takahashi* reasoning. In order to take into account all flux and torque variation possibilities, it is necessary to use a three state regulators for both flux and torque. This leads to 9 combinations of c_τ and c_ϕ. However, the one consisting of maintaining the flux and torque is not practically feasible. The remaining problem is how to coordinate between c_τ and c_ϕ? An approach to solve this problem consisting of [3] :

- in domains D_{m2}, D_{g2}, and D_{g4}, to increase the torque, a zero-voltage sequence is applied if $c_\phi = -1$ or 0. Else, an appropriate active voltage vector is used to increase the flux and tune the torque depending on c_τ.
- in domains D_{m1}, D_{g1}, and D_{g3}, to decrease the torque, a zero-voltage sequence is applied if $c_\phi = -1$ or 0. Else, an appropriate active voltage vector is used to increase the flux and tune the torque depending on c_τ.

Thus a new switching table, including two parts depending on the sign of the derivative of the torque with respect to time (domains D_{m2}, D_{g2}, D_{g4} for $\frac{d}{dt}T_{em} > 0$ and domains D_{m1}, D_{g1}, D_{g3} for $\frac{d}{dt}T_{em} < 0$), has been proposed as illustrated in table 4.

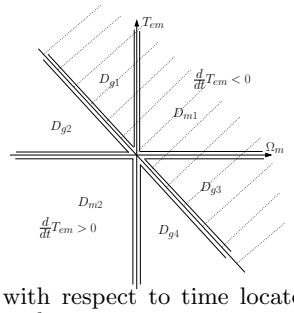

Figure 7: Torque variation with respect to time located in the torque-speed plane **Legend:** dotted area refers to $\frac{d}{dt}\ T_{em} < 0$, white area refers to $\frac{d}{dt}\ T_{em} > 0$.

Table 4: DTC look-up table depending on the torque variations.

c_ϕ	+1	0	-1	+1	0	-1	+1	-1
c_τ	+1	+1	+1	-1	-1	-1	0	0
Domains (D_{m2}, D_{g2}, D_{g4})								
S_1	V_2	V_0	V_0	V_6	V_6	V_5	V_1	V_0
S_2	V_3	V_7	V_7	V_1	V_1	V_6	V_2	V_7
S_3	V_4	V_0	V_0	V_2	V_2	V_1	V_3	V_0
S_4	V_5	V_7	V_7	V_3	V_3	V_2	V_4	V_7
S_5	V_6	V_0	V_0	V_4	V_4	V_3	V_5	V_0
S_6	V_1	V_7	V_7	V_5	V_5	V_4	V_6	V_7
Domains (D_{m1}, D_{g1}, D_{g3})								
S_1	V_2	V_2	V_3	V_6	V_0	V_0	V_1	V_0
S_2	V_3	V_3	V_4	V_1	V_7	V_7	V_2	V_7
S_3	V_4	V_4	V_5	V_2	V_0	V_0	V_3	V_0
S_4	V_5	V_5	V_6	V_3	V_7	V_7	V_4	V_7
S_5	V_6	V_6	V_1	V_4	V_0	V_0	V_5	V_0
S_6	V_1	V_1	V_2	V_5	V_7	V_7	V_6	V_7

5. Simulation

Simulation works have been carried out considering a sampling period $T_s = 50\mu s$. The flux and torque hysteresis bands have been taken $\varepsilon_\phi = 0.02$Wb and $\varepsilon_\tau = 3$N.m, respectively.
The load torque constant K has been calculated and has been found equal to whose 57.762N.m.
Referring to the experimental tests shown in figure 4, we have considered for every hour of the day, the orientation angle of the panels corresponding to the maximum no-load voltage (which represents the maximum sunshine position at that time). So the reference angle varies according to the following procedure:

- from 0s to 2s, the reference position is equal to 17.02 degrees corresponding to the maximum no-load voltage at 2PM. so the load torque is equal to 16.9 N.m,
- the reference position increases during 0.5 s to reach 29.68 degrees, corresponding to the maximum no-load voltage at 3PM. The load torque is equal to 28.6 Nm,
- from 2.5s to 4s, the reference position is kept constant equal to 29.68 degrees, so does the load torque.

In what follows the implementation of the previously-studied DTC strategies: (i) the *Takahashi* DTC basic strategy, (ii) the one based on the *Takahashi* DTC basic strategy where zero-voltage vectors have been discarded in the look-up table, and (iii) the one which takes into account the electromagnetic torque dynamic considering to four quadrant operation and leading to a dual look-up table. The obtained results are shown in figures 9 10 11.
Referring to figures 9-a, 9-b and 9-c which show the variations versus time of the position, the speed, and the electromagnetic torque, respectively, one can notice, on one hand, that the *Takahashi* DTC basic strategy offers high performance in transient and steady state operations. On the other hand, and referring to figure 9-d, one can notice the low performance of the *Takahashi* DTC basic strategy at low speed operation. Under such condition, and for steady state operation, the motor turns to be demagnetized as already expected in the previous section. At zero stator frequency and when a zero voltage vector is applied, the stator current causes a reduction of the stator flux magnitude. In order to overcome the problem of demagnetization caused by zero-voltage vectors included in the look-up table of the *Takahashi* DTC strategy, these have been substituted by active vectors. The obtained results are illustrated in figure 10. Referring to figure10-c, one can clearly notice that the problem of demagnetization has been discarded, while the motor high dynamic performance is not affected. Nevertheless, the torque ripple amplitude rises considerably with respect to the one yielded by the *Takahashi* DTC basic strategy, which represents a serious drawback.
Figure 11 shows simulation results obtained following the implementation of the third DTC strategy. These results highlight the high dynamical performance which are obtained with a low torque ripple amplitude and with the demagnetization discarded. Further investigation of the stator flux has been achieved

through the representation of the stator flux vector extremity locus in the (α, β) plane. This has been done considering the three DTC strategies. The obtained results are shown in figure 5.. One can clearly notice that the third DTC strategy yields the smoothest circular locus. For the sake of a deep comparison between the three studied DTC strategies, a third criterion has been taken into account, that is the average switching frequency F_c of the inverter power switches.
Figures 12, 13 and 14, show the average frequencies commutations of the inverter power switches, with (a), (b) and (c) represent the average frequencies commutations by first, second and third leg, respectively, and (d) represents the global average frequency correspond to figures 9, 10 and 11, respectively. Commutations frequencies of the inverter switches, with (a), (b) and (c) correspond to the cases of figures 9, 10 and 11, respectively. It is to be noted that the *Takahashi* DTC strategy and the analytically based one offer relatively low values of F_c compared to the modified *Takahashi* DTC strategy.

Following the investigation of the performances of the three studied DTC strategies, one can conclude that the analytically based DTC strategy represents a compromise which fulfills the three comparison criteria.

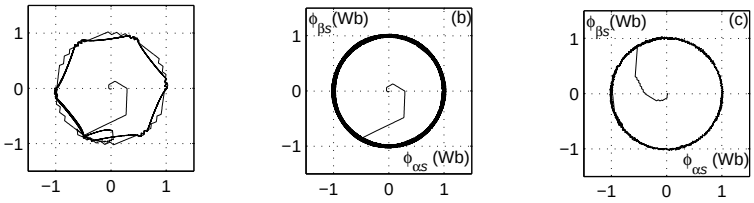

Figure 8: Locus of the extremities of $\overline{\Phi}_s$, with (a), (b) and (c) correspond to figures 9, 10 and 11.

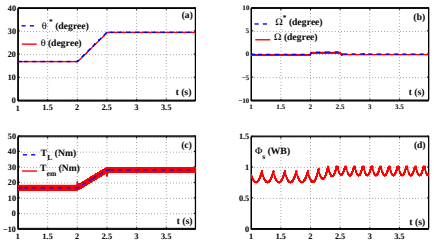

Figure 9: Position regulation by the implementation of the *Takahashi* DTC strategy, (a): angular position and its reference , (b): measured speed, (c):electromagnetic torque and load torque, (d): stator flux.

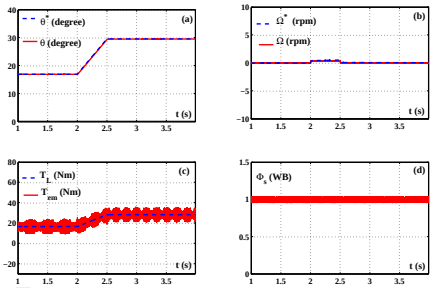

Figure 10: Position regulation considering a modified *Takahashi* DTC strategy, (a): angular position and its reference, (b): measured speed, (c):electromagnetic torque and load torque, (d): stator flux.

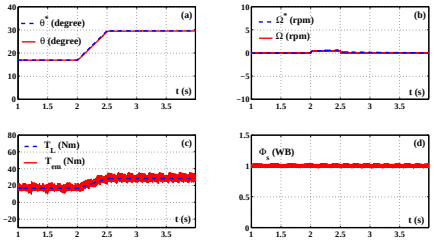

Figure 11: Position regulation considering an analytically based DTC strategy, (a): angular position and its reference, (b): measured speed, (c):electromagnetic torque and load torque, (d): stator flux.

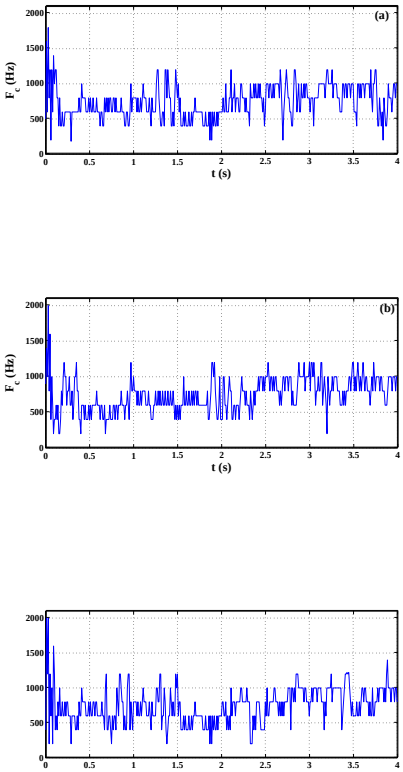

Figure 12: Average frequencies commutations of the inverter power switches, with (a), (b) and (c) : average frequencies commutations by first, second and third leg respectively, and (d) : global average frequency correspond to figure 9

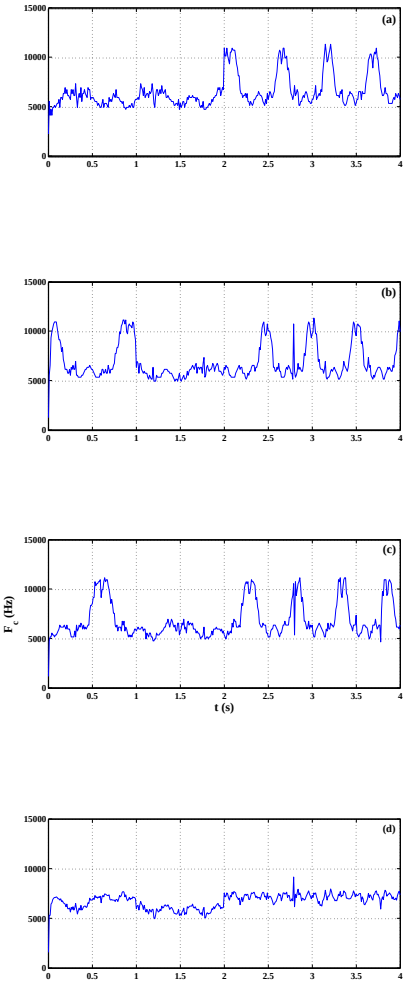

Figure 13: Average frequencies commutations of the inverter power switches, with (a), (b) and (c) : average frequencies commutations by first, second and third leg respectively, and (d) : global average frequency correspond to figure. 10

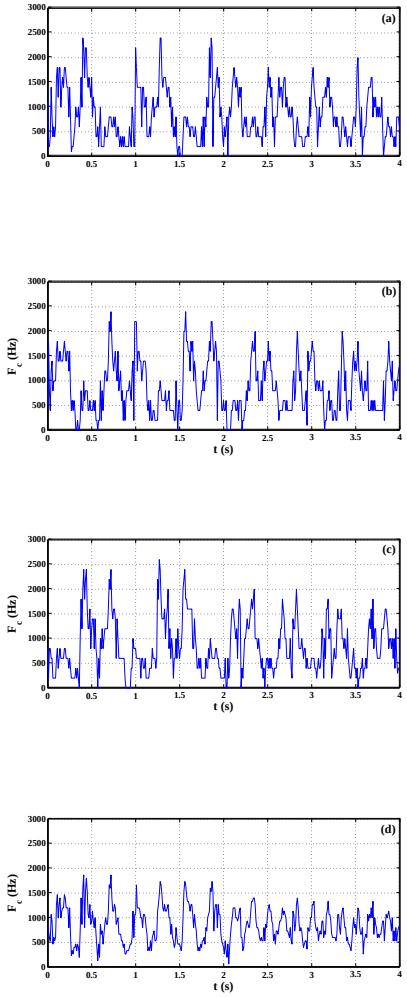

Figure 14: Average frequencies commutations of the inverter power switches, with (a), (b) and (c) : average frequencies commutations by first, second and third leg respectively, and (d) : global average frequency correspond to figure. 11.

6. Conclusion

This paper propose an approach consisting in moving photovoltaic panels according to the maximum sunshine position to allow a high efficiency of photovoltaic systems. The model of the photovoltaic generator is described. A new maximum sunshine position tracking system is presented on which three photovoltaic Siemens panels (SM100) were fixed. Some experimental measurements, consisting of no-load voltage, have been carried out using this built test bench. This tests allowed the creation of a data base that has been exploited for the resolution of the problem of maximum sunshine position tracking. Then, the paper proposed a comparison between three DTC strategies: (i) *Takahashi* strategy, (ii) the strategy based on the *Takahashi* one where zero-voltage vectors have been discarded in the look-up table, and (iii) the one which takes into account the electromagnetic torque dynamic considering four quadrant operation leading to a dual vector selection table. Referring to the simulation results, It has been found that the second and the third DTC strategies exhibit better transient behavior than the first one. Indeed, at low speed, *Takahashi* DTC strategy is penalized by the problem of demagnetization which is yielded by an oscillating flux response. Thanks to the application of active voltage vectors in place of the zero voltage one in the look-up table of the second strategy, the problem of demagnetization could be solved, however, this choice gives rise to an increase of the average inverter switching frequency and the torque ripple amplitude. To reduce both, the commutation frequency of the inverter power switches and the demagnetization phenomena, we have been found that the third DTC strategy is the best one. As a result, a reduction of the commutation losses in the inverter has been gained and the problem of demagnetization has been discarded.

References

[1] Takahashi I, Noguchi T. A New Quick-Response and High-Efficiency Control Strategy of an Induction Motor. *IEEE Trans. on Industry Applications* (IEEE Trans) 1986; vol. IA-16, pp. 820-827.

[2] Depenbrock M, Baader U, Gierse G. Direct Self-Control (DSC) of Inverter-Fed Induction Machine: a Basis for Speed Control without Speed measurement. *IEEE Trans. on Power Electronics* (IEEE Trans) 1988; l. 3, No. 4, pp. 420-429.

[3] El Hassan I, Roboam X, De Fornel B, Westerholt E V. Torque dynamic behavior of induction machine direct torque control in four quadrant operation. *Proc. IEEE ISIE'97 Conference* (ISIE'97) 1997; Lisboa/Portugal, pp. 1034-1038.

[4] Alfonso D, Gianluca G, Ignazio M, Aldo P. An Improved Look-up Table fo Zero Speed Control in DTC Drives. *Proc. European Conference on Power Electronics and Applications* (EPE) 1999; Lausanne/Switzerland, vol. 3, pp. 1-10.

[5] Msoum M A S, Dehbonei H, Fuchs E F. Theoritical and experimental analyses of photovoltaic systems with voltage- and current- based maximum power-point tracking. *IEEE Trans. on Energy Conversion* (IEEE Trans) 2002; vol. 17, NO.4.

[6] Ben Salem F, Yangui A, Masmoudi A. On the Reduction of the Commutation Frequency in DTC: a Comparative Study. *Proc. Transaction on Electric Power Engineering* (ETEP) 2004; Vol. 15, No. 6, pp. 571-584.

[7] Kolhe M, Joshi JC, Kothari DP. Performance analysis gf a directly coupled photovoltaic water-pumping system. *IEEE transactons on energy conversion* 2004.

[8] Mimouni MF, Mansouri MN, Benghanem B, Annabi M. Vectorial command of an asynchroous motor fed a photovoltaic generator. *Renewable energy* (ELSEVIER) 2004; No. 29, pp. 433-442.

[9] Vorobiev P Yu, Hernandez J G,Vorobiev Y V. Optimazation of the solar energy collection in tracking and non-tracking photovoltaic solar system. *1st international Conference on electrical and electronics engineering*(IEEE) 2004.

[10] Koutroulis E, Kalaitzakis K, Tzitzilonis V. Development of an FPGA-based System for Real-Time Simulation of Photovoltaic Modules. *Seventeenth IEEE International Workshop on Rapid System Prototyping* (RSP'06) 2006.

[11] Bouzidi B, Ben Salem F, Yangui A, Masmoudi A. Direct Torque Control Strategy Based Maximum Sunshine Position Tracking. *International Conference on Ecologic Vehicles and Renewable Energies* (EVER) 2007; Vol. 15, No. 6, pp. 571-584.

[12] Chenni R, Makhlouf M, Kerbache T, Bouzid A. A detailed modeling method for photovoltaic cells. *energy* (ELSEVIER) 2007; No. 32, pp. 17241730.

Biographies

Badii Bouzidi was born in Ksour-Essef, Tunisia, in 1981. He received the BS degree in 2005 in electromechanical engineering, and the MS in 2006 in electrical engineering, both from the Sfax Engineering School (SES), University of Sfax, Tunisia. He is currently preparing his PhD degree in electrical machine drives. He has been a contractual assistant in the Informatics High Institute of MAHDIA since 2006. Mr Bouzidi is a member of the Research Unit on Renewable Energies and Electric Vehicles of the University of Sfax, BP W, 5180 ksour-Essef, Tunisia. E-mail:badiibouzidi2010@yahoo.fr

Abderrazak Yangui was born in Sfax, Tunisia in 1956. He received the B.S., the DEA degree and the PhD degree in Electrical Engineering from the Sfax Engineering School (SES), University of Sfax, Tunisia in 1982, 1992 respectively. From 1982 to 1992 he was an Assistant Professor in the Electrical Engineering Department of (SES). Since Mars 1992 he has been an Associate Professor at the same university. His main research interests cover several aspects related to machines, electronic power and control.

Fatma Ben Salem was born in Sfax, Tunisia, in 1978. She received the BS and the Master degrees in 2002 and 2003, respectively, both in electrical engineering from the Sfax Engineering School (SES), University of Sfax, Tunisia. She is currently preparing her PhD degree in electrical machine control. Miss Ben Salem is an assistant professor of electrical engineering at the High Institute of Industrial Management of Sfax, Tunisia. She is a member of the Research Unit on Renewable Energies and Electric Vehicles of the University of Sfax. Her major interests are field oriented and direct torque controls of induction motors.